MSc in Photonics

PHOTONICS**BCN**

Universitat Politècnica de Catalunya (UPC)
Universitat Autònoma de Barcelona (UAB)
Universitat de Barcelona (UB)
Institut de Ciències Fotòniques (ICFO)

http://www.photonicsbcn.eu

Master in Photonics

MASTER THESIS WORK

OBSERVING THE ANGULAR RADIATION PATTERNS OF SINGLE EMITTERS BY BACK FOCAL PLANE IMAGING

Dimitrios Karanikolopoulos

Supervised by Prof. Dr. Niek F. van Hulst, (ICFO)

Presented on date 9th September 2013

Registered at

Escola Tècnica Superior d'Enginyeria de Telecomunicació de Barcelona

Observing the angular Radiation Patterns of Single emitters by Back Focal Plane Imaging

Dimitris Karanikolopoulos

Molecular Nanophotonics Group, ICFO-The Institute of Photonic Sciences, Mediteranean technology Park, 08860 Castelldefels(Barcelona), Spain

E-mail: dimitris.karanikolopoulos@icfo.es

Abstract.

This study is concerned with the fluorescence of single quantum emitters. The emission patterns of these emitters are affected by their environment. We modify the inhomogeneous environment of single emitters using near-field scanning optical microscopy. Our set-up allows for high positioning accuracy, to approach an antenna probe within the near-field of quantum dots and fluorescent beads. To gain insight on these changes, we access the angular information of the fluorescence from these emitters using the technique of back focal plane imaging. We show changes in their emission patterns as the field is dictated by the antenna modes. Analysis of the angular emission patterns of single molecules determine their three dimensional orientation. This method is advantageous compared to previous experimental approaches, since it facilitates data analysis due to the simple analytical form used to express the radiation patterns.

PACS numbers: Nano-optics, single molecules microscopy, optical antennas

1. Introduction

Electronic states of single molecules can be modeled as electric dipoles. A quantum source described this way has well defined absorption-emission properties such as atomic-like scattering cross-section, transition rates and angular distribution of the radiation pattern. Inhomogeneous environments alter these properties [1].Among the variety of engineered inhomogeneous environments, the use of optical antennas is one of the main used approaches during the last decade. These optical antennas, inspired by radio-frequency analogues, allow for sub-diffraction limited interaction with this kind of quantum emitters. They allow the retrieval of emitter properties and tailored modification of them.

More in detail, the study of single emitters mainly consists of the observation of the emitted fluorescence under illumination by highly focused fields which optimize the light-matter interaction [2]. By bringing nanostructures, as nanoantennas, in their vicinity, we access the emission components in the near-field which do not contribute to the radiated far-field [3], thus unveiling hidden information of the emission. In addition single emitters coupled to antennas radiate through the antenna modes, thus allowing for engineering of complex emission features [4].

To achieve efficient interaction between antenna and emitter both dynamic and static methods have been used. The former, rely on keeping either sample or scanning tip in a stable position while the other object is scanned with respect to it(NSOM, AFM). The latter scheme, consists of positioning the emitters near the antennas at

predetermined positions and subsequently irradiating the structure. These methods suffer from a certain positioning uncertainty in the first case and an unknown exact number of emitters placed close to the antenna in the second case. The ultimate control over the coupling between antenna and quantum emitter emitters would find application in many areas as are nanoscale imaging and spectroscopy[5-8], photovoltaics [9, 10], lithography[11], sensors[12, 13], single photon superemitters[14], nonlinear signal conversion[ref] and many more.

In this study, we present emission patterns of single quantum emitters directed through a nanorod antenna dynamically positioned over each individual emitter. We observe the alterations in the angular emission of quantum dots and fluorescent beads as their emission is directed by the antenna. In a second experiment we will gather the information about the angular dependencies of the radiation pattern using momentum space microscopy. This will let us to deduce the orientation of single molecules.

To dynamically position the antenna close to the emitter, we make use of a novel near-field optical microscopy(NSOM) set-up. The set-up is capable of moving both emitter and scanner tip with nanometer accuracy. This way deterministic positioning and coupling of each single emitter to the scanning antenna tip is achieved. The resulting fluorescence emission is recorded at the exit pupil of the optical system by projecting the back focal plane of the objective lens onto a camera detector.

This paper is structured as follows. We start by introducing the basic concept of how an optical antenna works. Second, we present the technique used to extract information about the angular distribution using back focal plane imaging. After that, we proceed explaining the actual method implementation used to place the antenna close to the emitters, as well as the optical set-up used to record the images in the back focal plane. Following we present the obtained results in three separate sections. We begin showing emission patterns of quantum dots and fluorescent beads in absence of the antenna. These emission patterns show an isotropical behaviour. In the second part deals with single molecule emission which is not isotropic. Using back focal plane(BFP) imaging we can determine the orientation of each molecule via its angular radiation pattern. No complicated data analysis is required for this purpose. On the third part we modify the angular distribution of the emission from nanoscale sources using antennas. The changes are studied using the previously described technique of BFP. Finally, conclusions about the properties of light sources at the nanoscale, and their interaction with subwavelength objects, are presented based on the analysis of the paper.

2. Optical Antennas

Optical antennas control light-matter interaction at the nanoscale and provide fundamental tools for Nano-optics. Their small size, on the order of the wavelength accounts for their properties. These properties include: enhanced localized fields to which the emitter couples. This due to the plasmoninc behaviour of the metals used for their fabrication. The antenna modes are in turn coupled to the radiation field and determine the angular emission of the coupled system. This is shown in figure 1(b), where a dipole emitter coupled to a dipole antenna .

By coupling an emitter to the antenna modes we enhance the local field and convert it to propagating radiation, whose directionality is dictated by the antenna structure. By reciprocity, propagating fields will be converted to localised energy at the antenna modes which enhance the excitation field. Realization of efficient optical antenna devices enable us to interface between propagating radiation and local sources [3].

3. Experimental

3.1. Back Focal Plane

In optics, the back (rear) focal plane of an optical system is the plane transverse to the rear focal point of the system. Rays that enter the system parallel to the optical axis z will cross at the back focal plane. Moreover, the scalar field at the back-focal-plane of any lens, is directly related to the Fourier transform of the object before the lens, $E(x, y : z) = \iint_{-\infty}^{\infty} \hat{E}(k_x, k_y; z) \exp^{i[k_x x + k_y y]} \mathrm{d}k_x \mathrm{d}k_y$. Each point on the object plane before the lens (x, y), is mapped into its reciprocal (k_x,k_y) in momentum space on the back focal plane [15].

This fact is of great interest to us because, from it ensues that the Fourier space image contains the directions of emission of the emitter. In addition, the intensity distribution in k-space, is related with the angle θ of inclination when vectorial fields are considered. The relation between each wavevector and the angle between the emitter dipole moment and optical axis can be extracted using fairly simple expressions. The coordinates on a back focal plane image, r (see figure 1(c)), are related to the inclination angle by: $r = Ksin\theta$, where K, a constant correlated with the magnification of the system. The intensity in turn, is related to the angular pattern by: $I(\theta, \phi) = I_{bfp}(k_x, k_y)cos(\theta)$, where $k_x = Krsin(\theta)cos(\phi)$ and $k_y = Krsin(\theta)sin(\phi)$ with ϕ being the azimuthal angle in the back focal plane and r the radial distance from the optical axis. The cosine factor is an apodization factor, introduced to conserve the energy along each path.

At this point it is essential to introduce the main factor which influences the shape of the obtained radiation patterns and requires for use of near-field optical microscopy for their study. Consider the case where a field propagating in a medium, finds the interface of a less dense medium. Within the context of the angular spectrum representation, rays travelling with an inclination angle larger than that of the critical angle ($\theta > \theta_{crit}$),which on the far field approximation have transmittion equal to zero, can take complex values. This practically means that evanescent waves are transformed into travelling waves.

The implications of this phenomenon are twofold, depending on the direction of the incoming field with respect to the layered system. We distinguish two scenarios. First, the case where the incoming field, emitted by a localized source, travels from a medium

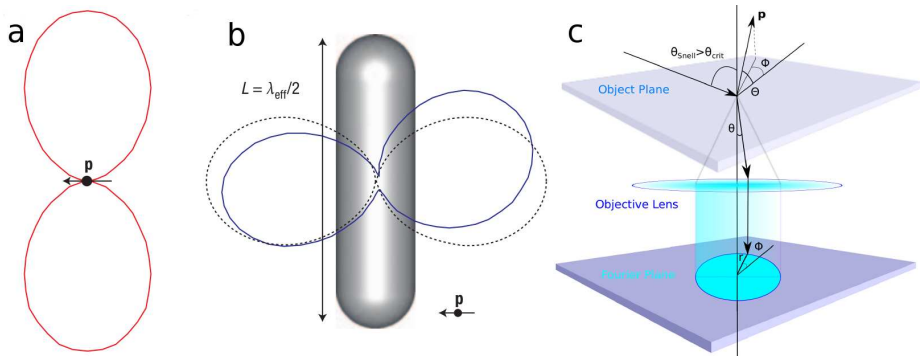

Figure 1. Emission control with a dipole antenna. **a**, Angular emission of a horizontal radiating dipole (**p**) in free space; **b**, Angular emission of the same dipole coupled to a vertical dipole antenna (blue), which has a length, L equal to half the effective wavelength at resonance, λ_{eff}, is dominated by the antenna (black dotted) (from [7]) **c,** Coordinate system used: Where **p**, the dipole moment.

with low index of refraction into another of larger. Waves whose k-vectors have an angle larger than the critical one (predicted for this interface($n_1 < n_2$ and $\theta > \theta_{crit}$)), have a finite transmission as opposed to the far-field case. Under these circumstances, the denser medium will bend the incoming radiation, which will propagate towards angles beyond θ_{crit}. This part of the radiation is referred to as *forbidden light* [16]. In a second scheme, the evanescent field created by light traveling from a medium of high refractive index finds the interface of smaller density. Fields whose k-vectors travel with angles larger than the critical($n_1 > n_2$ and $\theta > \theta_{crit}$) generate evanenscent components at the interface. These evanenscent fields, that exponentially decay away from the interface, can be converted into propagating radiation in a third medium. Provided the medium has a refraction index larger that n_1 ($n_2 < n_3 < n_1$)and is brought at such a distance near the interface in which the evanescent fields have not yet decayed. This phenomenon is called *frustrated total internal refraction* (FTIR) [17].

The main goal of this thesis was to build an optical set-up, which can project the back focal plane of the objective lens onto the active area of a CCD chip. This kind of optical system is referred to as a conoscope (figure 3), and its operation is as follows. A tube lens collects the photons gathered by the objective lens. These photons are propagating along the optical axis. A set of lenses projects an intermediate image object onto the detector area, thus forming the real plane image. The conjugated Fourier plane is relayed along with the real plane image. By positioning another lens, known as a Bertrand lens, between the relay optics and detector we can project a Fourier plane image onto the detector area. This way, the angular distribution of emitted light is recorded, enabling us to directly observe changes in the angular emission of quantum emitters when brought close to nanoscale objects. In the case of a single dipole emitter oriented parallel to a glass substrate, the intensity distribution in $k-$space forms a double lobed pattern(figure 2(a)). This is due to the effect of the substrate in the vicinity of the emitter. The donut mode of the single dipole crosses the substrate transversely in two regions that are symmetrical with respect to the dipole axis. The substrate converts the near field radiation into propagating fields which travel beyond θ_{crit} to form the angular pattern in the Fourier plane. These changes in angular emission, due to the existence of the substrate, are highly dependent on the distance of the dipole from the substrate and its respective angle with the $z-$axis vertical to the in plane directions x, y.

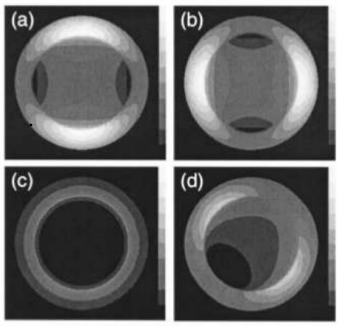

Figure 2. Calculated emission patterns of a dipole at an air-glass interface in the back-aperture plane of a NA 1.4 objective lens: **a**, $\Theta = 90°$, $\Phi = 0°$ (horizontal dipole); **b**, $\Theta = 90°$, $\Phi = 90°$ (horizontal dipole); **c** $\Theta = 0°$, $\Phi = 0°$ (vertical dipole); **d**, $\Theta = 45°$, $\Phi = 45°$ (from [18]).

3.2. Near-Field

Our set-up utilizes an Ar-Kr gas laser (Innova 70c spectrum) at $\lambda = 647nm$ fed into a Zeiss Axiovert 135 TV inverted microscope, figure 3. Before entering the microscope, the collimated beam is propagated through a series of polarization optics which enable

us to use either linear or circular polarized light to excite our sample. The beam focused on the sample using a high NA-oil immersion microscope objective (Zeiss Fluar $100x/1,30$NA). The same objective collects the emergent, stokes shifted, fluorescence emission signal.

To be able to witness the effect of the antenna on the emitter, we use a home-built NSOM set-up. This set-up enables us to exert control over the mutual position between the emitter and the scanning tip within the optical axis of the microscope [19]. The NSOM head is equipped with a three dimensional piezoelectric scanner bearing the antenna probe (figure 3). In order to maintain the antenna tip within the near-field of the emitters, the vertical direction of the NSOM head is controlled by a Shear Force Feedback mechanism [20]. Combined with the piezoelectric stage on which the sample is placed it gives us a total of five directional degrees of freedom over the sample-tip system.

We use three different types of emitters. Quantum dots (Invitrogen Evidot 850) and TDI molecules are embedded in a thin layer of PMMA (Poly(methyl methacrylate)) and fluorescent beads (Invitrogen F-8783) embedded in PVA(Polyvinyl alcohol). Samples are made spin coating the polymer containing the emitters onto cleaned cover slips. The average size of each type of emitters is $\leq$ 10nm for the quantum dots, 20nm for the beads and $\sim$ 1nm for single molecules. All used emitters feature a broadband excitation spectrum which can be directly excited by our laser beam and an emission peak around 680nm. The collected signal passes through a dichroic beam splitter in order to separate it from the excitation field. Before the signal is detected, it is further filtered using a long pass filter that rejects the laser light by over 5 orders of magnitude. This ensures no excitation light is present in the detected signal.

There are two available detection branches in our microscope. We can direct the signal in either one, by inserting a mirror in the optical path of the beam. Both optical

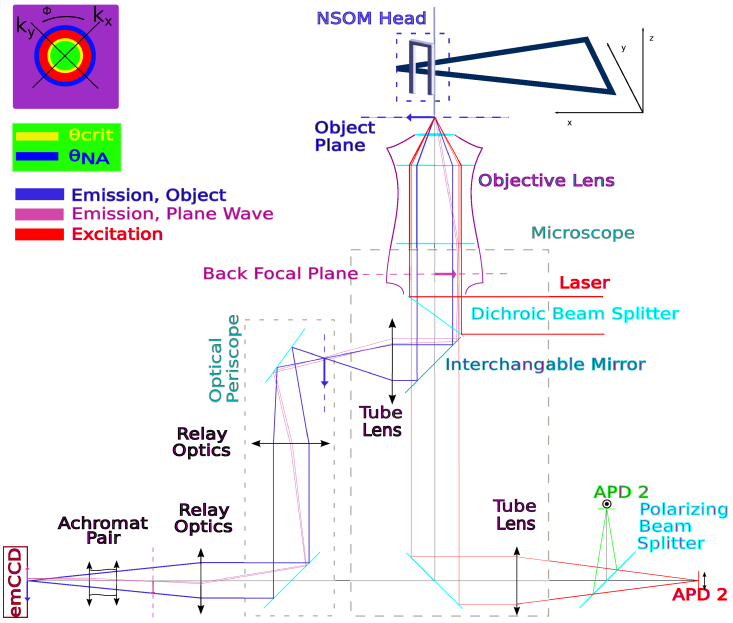

Figure 3. Set-up: The two detection branches are displayed. The back focal plane set-up for angular detection is shown on the left and the one for confocal imaging on the right. The respectfull elements are marked on the sketch. The inset shows the form of a back focal plane image.

paths feature a tube lens that redirects detected light out of the microscope. The first detection branch allows for confocal imaging of the raster scanned sample. The emission fluorescence is guided through a polarizing beam splitter cube which divides the collected photons in two orthogonal polarizations. The two signals are then detected by focusing them on two separate avalanche photodiodes. The other branch of our microscope, features the configuration of optical elements combined in order to form the back focal plane onto our camera detector, following the reasoning of the previous section.

Since the main purpose of this thesis was to build a BFP imaging system compatible with the NSOM microscope, further insight is given on this part of the set-up. An optical periscope was used to direct the beam from the exit port of the microscope to the optical table, where an electron-multiplied CCD (emCC)(Hamamatsu ImagEM C9100-13) is located. Two pairs of plano–convex lenses featuring different focal lengths where used. The first pair of lenses act as relay optics used to create an intermediate image of the Fourier plane in the space between the lower part of the periscope and the detector area of the camera. The other two lenses are combined to form an achromat pair which is used to image this plane on the emCCD camera.

In detail, an achromat pair refers to a combination of two plano–convex lenses of equal focal lengths, placed with their curved surfaces facing each other and separated by a distance less than their focal length. This results in a spreading of the focusing power of the system of two lenses, allowing us to focus the detected signal using lenses with longer focal distances. The smaller the focal length, the more aberrations are introduced in the optical system, which we want to avoid by any means. Even more, since lenses introduce spherical aberrations, the facing-off second lens compensates for the aberrations introduced by the first one. The pair acts then as one lens featuring an equivalent focal length dictated by the relation: $EFL = (f_1 \cdot f_2)/(f_1 + f_2 - d)$, where f_1, f_2, d are the focal lengths of the respective lenses and d their mutual distance. In our case where $f_1 = f_2 = d = 100mm$ we obtain an $EFL = 100mm$. Using the aforementioned emCCD detector is advantageous for detecting the signal arising from single quantum emitters, since it multiplies the signal of each photon gathered, reducing the background. This results in a significant improvement of the signal to noise ratio; an important parameter when low intensity signals are being detected, as is our case.

To be able to make a good BFP imaging system we must overcome a set of technical difficulties of such optical set-ups as well as achieve optimal calibration. This has to be done within the constraints of our space on the optical table. One of the factors mainly affecting our system is optical aberrations. These are induced in the beam by the lenses, whose limited collection angle and imperfect manufacturing result in spatial-frequency filtering. Moreover, if the beam, does not pass from the center of the lenses, or leaves the mirrors in angles which are not normal, inducing coma aberration that degrades the quality of the images in the momentum space.

Calibration of the momentum space images was achieved using diffraction gratings. Misalignment in any part of the set up, would introduce additional shapes in our image of the diffraction orders of the grating in $k-$space, or blur the imaged signal. Moreover, the lenses must be correctly selected and fine tuned as to project the intermediate Fourier plane on the detector area. Lenses of large($\geq 200mm$) focal lengths result in long set ups, necessitating for more space on the optical table, while those of short focal lengths($\sim 50mm$) induce substantial aberrations; because sharp angles are required to bend the beams enough to focus them at the focal spot. If the distances between the lenses are not correct we can see a mixture of Real and Fourier planes while calibrating with the diffraction grating. If we image the radiation pattern at this point,

its boundaries will not be sharp enough and the separation between the outer and inner region will not be as discontinuous as that of a clear Fourier plane image. A second parameter that needs to be taken account is that the initial image on the back focal plane of our objective needs to be properly magnified to fit the camera chip size. It should be such that, on one hand, results in the formation of a pattern large enough to be able to study properly, while on the other hand, not to large, as this would result in the signal being spread on a large area over the CCD chip. This would lead to low photon counts at each point(pixel).

In the final configuration of the setup implemented during this master project, the sample was excited with an intensity analogous to $1\mu W$ (usually less in order to avoid photobleaching of the emitters in the sample). The angular radiation pattern of the emission(units: Power density per unit solid angle), containing information on the intensity distribution was projected over approximately 140×140 pixels, accounting for a magnification of M=0.56. The intensity was recorded over 20 seconds, in 20 accumulation steps of 1 second. The measurement was performed using an antenna tip positioned over each bead. In the case of single molecules we acquired the fluorescence over 10 seconds, in 10 accumulation steps of 1 second.

4. Results

4.1. Radiation patterns of quantum emitters

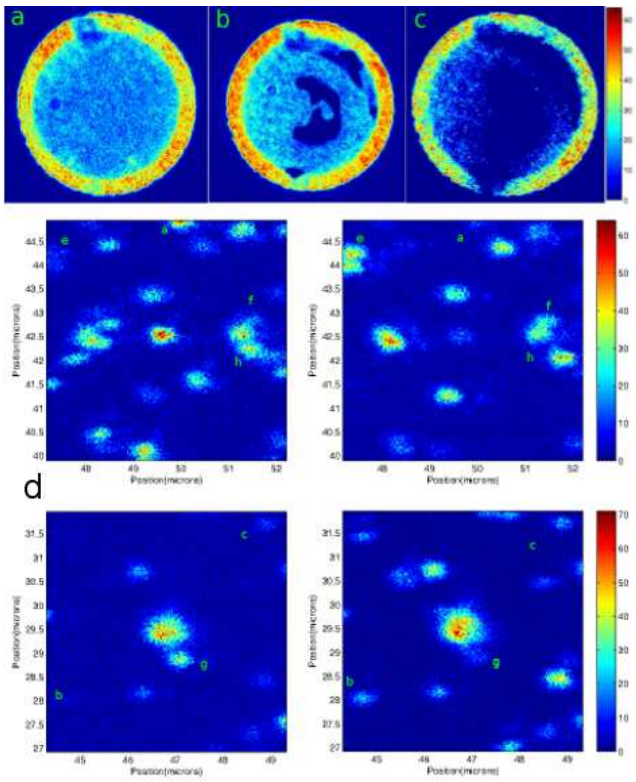

Figure 4. Radiation patterns and Confocal images a, Quantum Bead; **b,** Fluorescent Bead; **c,** Fluorescent bead coupled to the antenna tip; **d,** Confocal images for both in-plane polarizations, x left and y right.

To get a feeling of the experiments involved, we start studying the emission from

samples containing fluorescent beads or quantum dots. For both samples we expect to see an isotropic emission. Quantum dots are known to emit isotropically. This is due to the fact that these nanocrystals have degenerate transition dipole moments oriented in a bi-dimensional plane and thus exhibit no prefered emission direction[21-24]. As regards to the beads, since the fluorescent molecules constituting them are randomly oriented, we should induce excitation and emission in all directions. We excite the sample using a circularly polarized beam. This way we are certain to excite all the dipole transition moments present in each of the emitters, irrespective to their orientation in space.

The obtained results coincide with the previously established theory (figure 2) [18]. The recorded angular radiation patterns are characteristic of isotropic emitters[figure 4]. These patterns contain the information of the momentum space($k-$space) and have two characteristic circular borders forming a ring on the outer part of the pattern[see inset of figure 3]. The outer circle is the limit posed by the maximum collection angle of our objective lens ($\theta_{NA} = 58.79°$) and the inner that of the critical angle at the glass air interface ($\theta_{crit} = 41.1°$). Within this region, beyond θ_{crit}, the intensity is larger than that in the center of the pattern: *forbidden light* is more intense than *allowed light* [25]. Since both quantum dots and beads emit in all directions, both their patterns have their intensity distributed in all the angles, forming a uniform distribution of intensity within the ring.

4.2. Single molecule orientations

For this part of our study, we analyse the emission patterns obtained from 52 different molecules under confocal excitation. We make use of a circularly polarized laser beam which can excite all the in-plane orientations, thus achieving maximum excitation efficiency. For these measurements a higher NA objective lens was used(Zeiss, α Plan-Apochromat $100x/1.46$NA). The resulting images have a wider area formed between the critical angle and the new maximum collection angle ($\theta_{NA} = 72.8°$).

In figure 5, we compare the radiation patterns of seven different molecules accounting to an equivalent number of dipole orientations and correspond to the labeled positions in the confocal images found in figure 4(d). The power of the method used to obtain the radiation patterns, can be seen in the recorded images. We can extract qualitative information regarding the orientation of these dipoles with respect to the substrate by careful interpretation of the recorded intensity distribution.

The orientation of the dipoles are represented by their polar and azimuthal angles (Θ, Φ) with respect to the $x-$ and $z-$ axis as defined in figure 1(c) (also shown in figure 5(d)). Clear images of the double lobes for molecules situated in-plane with the substrate($\Theta = 0°$) are shown in figure 5 (a), (b) and (e). These correspond to in-plane x direction ($\Phi = 0°$), in-plane y direction ($\Phi = 90°$) and the intermediate angle, ($\Phi = -45°$). These results are in agreement with the confocal fluorescence images of these single molecules. Molecule (a) appears only in the in-plane confocal image, (b) only in the out-of-plane [figure 4(d)].

Patterns (c),(f),(g) and (h) ensue from dipoles oriented out-of-plane i.e. dipoles with an angle $\Theta \neq 0°$ between substrate and the out-of-plane $z-$axis. The extreme case of dipole oriented perpendicular to the substrate($\Theta = 90°$) is shown in (c) and is that of an isotropic emitter. The donut-shaped pattern of the dipole is parallel to the surface, and thus equal signal is detected in all the angles, resulting in the ring shaped pattern.

The angular patterns of molecules (f), (g) and (h) are not as straightforward to interpret. As experimental results have shown, the radiation pattern changes

when a dipole is oriented with an angle between the in-plane(horizontal) and out-of-plane(vertical) direction. To describe this situation we consider the dipole being a vector in spherical coordinates, with one extreme fixed at the origin of the axes(see figure 5 (d)). As the other extreme(vector point) is raised from the x-y plane ($\Theta > 0$) more photons are gathered in the direction to where the extreme is out of plane, accompanied with detection of photons in the central area of the pattern, below θ_{crit}. This results in a higher intensity of the lobes of these patterns towards the direction of the raised extreme of the dipole, while in the other direction a drop in the number of photons is observed.

These changes can be seen in molecule (f) and its antisymmetric to the $z-$axis (g). Both patterns show an angle $\Phi \sim 45°$ and resemble the pattern of molecule (e). However, the former molecule pattern displays an increased intensity in the right hand side, this is representative of molecules with angles $\Theta < 90°$(positive z component) . On the other hand, the latter molecule (g), shows increased intensity in the left hand side pointing to an angle $90° < \Theta < \pi$ (negative z component).

Very good agreement of the experimental results with the calculated emission pattern is accomplished in the case of molecule (h) . The pattern in (figure 2(d)) is antisymmetrical with respect to the $z-$axis. An angle $\Theta = 135°$ is accurately reproduced by the recorded data. The photons are unevenly distributed towards the left side with radiation gathering next to the main lobes as well as in the center of the pattern.

The last three results mentioned, highlight one of the advantages of this method, its ability to distinguish between molecules which exhibit mirror symmetry in the vertical axis.This is not possible with methods using polarization analysis to determine the orientations, [26]

4.3. Emitters coupled to an antenna tip

To achieve proof of principle of the efficient coupling of the antennas with the emitters we use our NSOM set up and bring an antenna tip ($L = 164.6nm$) probe close to the fluorescent beads. The antenna is fabricated at the apex of a fiber and its length is tuned to dipolar resonance with our driving radiation wavelength, $\lambda = 647nm$. By means of Shear force feedback we position and maintain the antenna at a distance

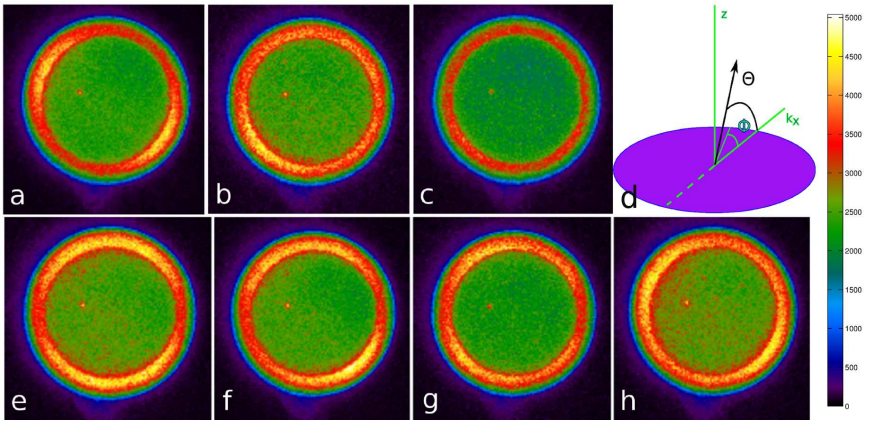

Figure 5. Comparison of the orientations of single molecules: **a**, $\Theta = 0°$, $\Phi = 0°$ (horizontal dipole); **b**, $\Theta = 0°$, $\Phi = 90°$ (horizontal dipole); **c**, $\Theta = 90°$, $\Phi = 0°$ (vertical dipole); **d**, Back focal plane coorinate system; **e**, $\Theta = 0°$, $\Phi = -45°$; **f**, $\Theta =< 90°$, $\Phi =\sim 45°$; **g**, $90° < \Theta < \pi$, $\Phi =\sim 45°$; **h**, $\Theta = 135°$, $\Phi = 0°$.

analogous to 15nm from the emitters, while the sample containing the beads is raster scanned below it. When coupling between the emitter and the antenna is achieved, the two hot spots of the excited first antenna mode appear in the APD which records the polarization parallel to the antenna axis. Once we have ensured that our tip is resonant we proceed by keeping our sample in a fixed position and scanning with the antenna tip over the beads. By switching the mirror to direct the excitation fluorescence into the conoscope, we were able to record the emission of the quantum sources redirected through the antenna. As we can see in figure 4(c), the recorded pattern has changed and the intensity is distributed in two lobes. This no longer corresponds to an isotropic angular pattern characteristic of the beads, and suggests that the emission is of dipolar nature; *the bead is emitting through the antenna*. This is a very important result as it is proof of the antenna functioning as an efficient converter of the coupled near field of the emitter, to propagating radiation in the far-field.

5. Conclusions

We have showed the power of the back-focal-plane imaging method used for determination of the direction of the fluorescence emission of quantum emitters. The BFP set-up that was built within the framework of this thesis, allowed us record and study the radiation patterns of single emitters in presence and absence of antenna probes. We were able to prove that single emitter radiation gets funeled by optical antennas, driving the far-field radiation of the emitters. Furthermore, it enabled us to extract the orientation information of single molecules. The simple model required to describe the obtained data offers significant advantage over previous methods proposed. Combined with high positioning capability provided by the featured NSOM setup, it provides an ideal experimental platform to study light-matter interactions beyond the diffraction limit.

Acknowledgments

I would like to acknowledge my Thesis Advisor Prof. Niek van Hulst for his trust, advice and continuous support throughout this project. I am grateful to Anshuman Singh, Pablo de Roque, Ion Hancu, Alberto Curto and Marta Castro for all the help and knowledge they have extended to me. I also thank all the members of the Molecular Nanophotonics group for the constructive discussions.

6. References

1. Purcell, E.M., *Physical Review*, **69,**(11 12, 681 (1946))
2. Lukas Novotny. Erik J. Sanchez, X. Sunney Xie, . *Ultramicroscopy* **71**, 21-29 (1998)
3. L. Novotny, N. F. van Hulst. *Nature Photon*, **5**, 8390 (2011)
4. A. G. Curto, T. H. Taminiau, G. Volpe, M. P. Kreuzer, R. Quidant, N. F. van Hulst, *Nature Commun* **4**, 1750 (2013)
5. Novotny L. *Phys. Rev. Lett.* **98** 266802 (2007)
6. L. Novotny and S. J. Stranick. *Annu. Rev. Phys. Chem.* **57**, 303 331 (2006)
7. E. Bailo and V. Deckert. *Chem. Soc. Rev.* **37**, 921 930 (2008)
8. E. Fort and S. Grasillon. *J. Phys. D* **41**, 013001 (2008)
9. Catchpole K R and Polman A. *Opt. Express* **16** 21793 2008
10. Atwater H A and Polman A. *Nature Mater.* **9** 205 2010
11. Sundaramurthy A, Schuck P J, Conley N R, Fromm D P, Kino G S and Moerner W E., *Nano Lett.* **6** 355 2006
12. Anker J N, Hall W P, Lyandres O, Shah N C, Zhao J and van Duyne R P.*Nature Mater.* **7** 442 2008
13. Svedendahl M, Chen S, Dmitriev A . *Nano Lett.* **9** 4428 2009
14. Farahani J N, Pohl D W, Eisler H J and Hecht B. *Phys. Rev. Lett.* **95** 017402 2005
15. Novotny, L.; Hecht, B. *Principles of Nano-Optics* Cambridge University Press: Cambridge and New York, 2006.
16. B. Hecht, D. W. Pohl, H. Heinzelmann, and L. Novotny, O. Marti and R. Moller, eds., **Vol.300** of *NATO Advanced Study Institute, Series (Kluwer,Dordrecht, The Netherlands, 1995)*, pp. 93 107
17. L. Novotny, *J. Opt. Soc. Am.* **14**, 91 104 (1997)
18. M. Andreas Lieb, James M. Zavislan, and Lukas Novotny. *JOSA B*, **21**, Issue 6, pp. 1210-1215 (2004)
19. A. Singh, Phd thesis proposal, ICFO(Barcelona) 2013
20. Ruiter, A. G., van der Werf, K. O., Veerman, J. A., Garcia-Parajo, M. F., Rensen, W. H.,and van Hulst, N. F. *Ultramicroscopy* **71**(1-4), 149 157 (1998)
21. Empedocles S A, Neuhauser R and Bawendi M G. *Nature* **399** 126(1999)
22. Koberling F, Kolb U, Potapova I, Phillip G, Basch. T and Mews A. *J. Phys. Chem* **B 107** 7463 7471 2003.
23. Brokmann X, Coolen L, Hermier J and Dahan M. *Chem. Phys.* **318** 91-98.(2005)
24. Early K T, McCarthy K D, Odoi M Y, Sudeep P K, Emrick T and Barnes M D. *ACS Nano* **3** 453-461 (2009)
25. L. Novotny. *J. Opt. Soc. Am.* **A 14**, 105 113 (1997)
26. J. T. Fourkas, *Opt. Lett.* **26**, 211 2 (2001)
27. Palomba, S. and Novotny, L. *Nano Lett.* **9**, 3801 1804 (2009)
28. Danckwerts, M. and Novotny, L. *Phys. Rev. Lett.* **98**, 026104 (2007).
29. Lippitz, M., van Dijk, M. A. and Orrit, M. *Nano Lett.* **5**, 799 802 (2005)